UC Davis
UC Davis Previously Published Works

Title

Rational Design of Potent and Selective Inhibitors of an Epoxide Hydrolase Virulence Factor from Pseudomonas aeruginosa

Permalink

Journal

ISSN

Authors

Kitamura, Seiya
Hvorecny, Kelli L
Niu, Jun
et al.

Publication Date

DOI

Peer reviewed

Rational design of potent and selective inhibitors of an epoxide hydrolase virulence factor from *Pseudomonas aeruginosa*

Seiya Kitamura[†], **Kelli L. Hvorecny**[‡], **Jun Niu**[†], **Bruce D. Hammock**[†], **Dean R. Madden**[‡], and **Christophe Morisseau**[*,†]

[†] Department of Entomology and Nematology, and UC Davis Comprehensive Cancer Center, University of California, Davis, One Shields Avenue, Davis, California 95616

[‡] Department of Biochemistry, Geisel School of Medicine at Dartmouth, 7200 Vail Building, Hanover, New Hampshire, 03755

Abstract

The virulence factor cystic fibrosis transmembrane conductance regulator (CFTR) inhibitory factor (Cif) is secreted by *Pseudomonas aeruginosa* and is the founding member of a distinct class of epoxide hydrolases (EHs) that triggers the catalysis-dependent degradation of the CFTR. We describe here the development of a series of potent and selective Cif inhibitors by structure-based drug design. Initial screening revealed **1a** (KB2115), a thyroid hormone analog, as a lead compound with low micromolar potency. Structural requirements for potency were systematically probed, and interactions between Cif and **1a** were characterized by X-ray crystallography. Based on these data, new compounds were designed to yield additional hydrogen bonding with residues of the Cif active site. From this effort, three compounds were identified that are 10-fold more potent toward Cif than our first-generation inhibitors and have no detectable thyroid hormone-like activity. These inhibitors will be useful tools to study the pathological role of Cif, and have the potential for clinical application.

INTRODUCTION

Pseudomonas aeruginosa is a ubiquitous opportunistic pathogen that infects various sites of the human body, including the lungs in patients with diseases such as chronic obstructive pulmonary disease and cystic fibrosis.[1] The bacterium is naturally resistant to a large range of antibiotics and can acquire additional resistance,[2] creating a pressing need for novel therapeutic approaches.

Among its strategies for subverting host defenses, *P. aeruginosa* targets the cystic fibrosis transmembrane conductance regulator (CFTR), an ion channel important for epithelial fluid transport, mucociliary clearance and mucosal immunity in the lung.[3] *P. aeruginosa* secretes

the CFTR inhibitory factor (Cif) that blocks the post-endocytic deubiquitination of CFTR and thus facilitates its lysosomal degradation.[4] Cif is a member of the α/β hydrolase family and has demonstrated epoxide hydrolase (EH) activity.[5] Using site directed mutations and inhibitors, we observed that Cif EH activity is critical for the inhibition of CFTR deubiquitination. However, the endogenous substrate and exact mechanism of Cif virulence remain unknown, and the mechanistic link between EH activity of Cif and deubiquitination of CFTR still remains speculative. The availability of potent and selective Cif inhibitors should thus help to better understand Cif pathobiology and to explore possible clinical applications.

We recently identified tiratricol as a moderate Cif inhibitor with an IC_{50} of 4.7 μM.[5b] This compound protects CFTR from both purified Cif protein and *P. aeruginosa* PA14 applied to polarized human airway epithelial cells.[5b] This suggests that inhibition of the EH activity of Cif could be a therapeutic approach to maintain CFTR levels on the surface of epithelial cells following *Pseudomonas* infection, thus permitting faster elimination of the pathogenic bacteria. However, tiratricol binds the endogenous human liver nuclear thyroid hormone receptor with sub-nanomolar affinity. In fact, tiratricol has a higher affinity than the endogenous thyroid hormone T_3 (triiodothyronine),[6] consistent with reports of severe side effects that led the FDA to suspend the availability of tiratricol.[7] Relatively low potency toward Cif and extremely high potency toward the thyroid hormone receptor thus limit the application of tiratricol for further biological studies and possible human clinical application.

To circumvent the limitations of tiratricol, in this report, we identified related compounds and studied the interactions required for Cif inhibition, using two complementary approaches: chemical modification and X-ray crystallography of inhibitor complexes. Based on the results from both approaches, we designed and synthesized compounds with improved potency toward Cif and with no detectable thyroid hormone-like activity in a transgenic reporter system.

RESULTS AND DISCUSSION

Initial screening based on the tiratricol structure

Initial screening of commercially available and synthetic[8] compounds similar to the tiratricol structure (Table S1) revealed **1a** (KB2115[9]) to be slightly more potent than tiratricol. While **1a** is also a ligand selective for the thyroid hormone receptor β,[9-10] **1a** does not contain any iodine atoms, in contrast to tiratricol (Figure 1). Given the potency and relative ease of analog synthesis, **1a** represents a better initial lead compound for medicinal chemistry approaches to improve its potency against Cif.

Probing the structural requirements of lead compound 1a for Cif inhibition

Based on the general structure of the Cif inhibitors shown in Figure 1, we explored the structural requirements of Cif inhibition by **1a** more rigorously. Compound **1a** analogs were synthesized using methods similar to the one previously described for thyroid hormone analogs as shown in Scheme 1.[11] Briefly, S_NAr reaction between a phenol **2** and compound

3 gave a diphenyl ether **4**. De-protection of a methoxy moiety by boron tribromide yielded a phenol **5**. The nitro group was then reduced into a primary amine **6** using sodium dithionite. Finally, an amide bond was formed by reacting the aniline **6** with acid chloride.

The requirement for the R_1 functional group was studied first (Table 1). Compounds with a primary amine (**6a**) or a nitro moiety (**5a**) still possessed inhibitory activity, although potency dropped approximately three-fold. Inhibitory activity was also modestly affected when the primary amine was replaced by an alkyl amide (**1b**, **1c**). The ethyl ester form of the lead compound (**1d**) was also slightly less potent than the free acid form (**1a**). The compound with an additional methylene moiety (**1e**) was as potent as **1a**, with the ethyl ester form (**1f**) having slightly lower inhibitory activity than the free acid form. These data suggest that the terminal free carboxylic moiety interacts only weakly with the enzyme. In further synthesis of analogs for this initial study, we encountered difficulty in purifying some of the analogs with free acid forms on R_1. Therefore, the malonate ethyl ester moiety was selected as R_1 for the purpose of determining structural requirements at other positions.

Results for the structural requirements of the R_2, R_3, R_4 and R_5 functional groups are shown in Table 2. When the hydroxyl moiety at R_2 was replaced either by hydrogen (**1g**) or methoxide (**1h**), these analogs failed to show inhibitory activity at 50 μM or 25 μM, suggesting that the hydroxyl moiety is critical for inhibitory activity and that a hydrogen bond acceptor is not sufficient for the interaction. Replacement of bromines on R_3 and R_3' with chlorines (**1i**) resulted in an approximately two-fold increase in activity. Removal of one of the chlorines (**1j**) led to a decrease in activity, reflecting the importance of the halide R_3 substituents.

Replacement of the R_4 isopropyl with a proton yielded the non-substituted compound (**1k**), which showed no inhibition at 50 μM, indicating that the substituent at R_4 is critical for potency. Replacement of the isopropyl moiety with bromine (**1l**), iodine (**1m**), trifluoromethyl (**1n**), or acetylene (**1p**) moieties did not change the potency of the compound. This suggests the existence of available space in the binding pocket of Cif that can be filled by an R_4 substituent of the appropriate steric volume, but that its exact chemistry is not precisely constrained. A compound with bromine at the R_5 position (**1q**) had potency much lower than the corresponding R_4 substituent (**1l**), but slightly greater than the unsubstituted compound (**1k**), reflecting greater selectivity at the R_5 position.

Replacing the R_4 isopropyl moiety with a trifluoromethyl moiety (**1n**), which is a strong electron withdrawing group, increases the acidity of the phenol on R_2. Thus we expected that compound **1n** would form stronger hydrogen bonds, leading to higher inhibitory potency. However, compared to **1i**, the potency of **1n** did not improve dramatically.

Cif:1a structure

In parallel with our SAR studies, we determined the X-ray crystallographic structure of Cif complexed with lead compound **1a** at a resolution of 1.65 Å (Figure 2A, Table S2, Figures S1 & S2). The resulting model revealed that **1a** occludes access of the substrates to the catalytic pocket (Figure 2B). In general, the structure confirmed the findings from our medicinal chemistry approach. For example, the structure showed that the R_1 moiety is

located outside of the active-site tunnel and is not critical for the interaction with Cif (Figure 2B), consistent with our SAR data showing that changes in the R_1 chain have little effect on Cif inhibitory potency (Table 1). The structure also showed that the hydroxyl moiety at the R_2 position forms a hydrogen bond with the main-chain carbonyl oxygen of Gly270 (Figure 2). This supports our observation that removing this hydroxyl moiety resulted in great loss of potency (Table 2). One of the bromines (R_3) is close to the hydroxyl of Ser173 and the main-chain amide nitrogens of Leu174 and Val175, while the other bromine (R_3') is close to the thioether of Met272, indicating potential interactions between the halogens and these residues (Figure S3).[12] In addition, the dibromophenyl ring of compound **1a** appears to form a π-stacking interaction with Phe164, which may be strengthened by halogen substituents (Figure 2B).[13] The catalytic cavity opens around the isopropyl moiety of **1a**, indicating that larger groups could be present at position R_4, as we observed with our medicinal chemistry approach (Table 2).

The structural requirements of Cif inhibitors overlap with those of thyroid hormone receptor ligands[10a] at several positions. Tiratricol and **1a** reflect the intersection of these requirements, and thus serve as both thyroid hormone mimics and Cif inhibitors.[5b] For example, the hydroxyl group on R_2 and two halogens on R_3 & R_3' are required in both cases, and a bulky substituent is preferred on R_4. In the case of the thyroid hormone receptor, the terminal free acid of R_1 forms hydrogen bonds (Figure S4). On the other hand, the terminal free acid is not required for Cif inhibition (Table 1). Therefore, compounds with different R_1 groups were screened to evaluate their thyroid hormone activity.[14] The compound with propyl amide (**1c**) showed the lowest thyroid hormone activity while still effectively inhibiting Cif (Table S3, Figure S5). Therefore, the propyl amide moiety was selected as the R_1 moiety for further structural optimization.

Comparison to mammalian EH and their inhibitors, and inhibitor design strategy

In the case of mammalian epoxide hydrolases, urea and amide moieties are known to function as transition state analogs.[15] These moieties bind to the catalytic site very tightly by interacting non-covalently with the catalytic nucleophile Asp and the accessory Tyr-Tyr pair, leading to potent inhibition of these enzymes.[15a, 15c, 16] Cif has a conserved EH catalytic triad consisting of residues Asp129, Glu153 and His297, while it uses a non-canonical His177-Tyr239 accessory pair to coordinate the epoxide oxygen during ring opening.[5c] Based on the similar active-site chemistry, we expected that urea or amide functionalities could also interact with the catalytic site of Cif. However, simple alkyl urea/amide/carbamate compounds failed to show Cif inhibitory activity at 50 μM, as did a series of additional potent mammalian EH inhibitors with urea or amide pharmacophores (Table S4). The differential sensitivity of the mammalian and bacterial EHs is consistent with our previous discovery that they differ in the relative kinetics of formation vs. hydrolysis of a covalent intermediate[17], and suggests that the fine details of the transition states of the two EH families are distinct.

In the Cif:**1a** complex structure, an acetate ion was found in the catalytic site of the enzyme (Figures 2B and 2C), which was crystallized in a buffer containing sodium acetate. The active-site hydrogen bonding network includes interactions between the acetate ion and the

catalytic site residues Asp129, His177 and Tyr239 (Figure 2C), replicating many of the interactions of the local water network observed in the apo structure (Figure 2D). The distance between the isopropyl moiety and the acetate is roughly 4.5 Å (Figure 2B). The theoretical distance between the carbonyl and phenyl ring in compounds that have a phenyl carbonyl moiety at the R_4 position is approximately 4.3 Å, indicating that a phenyl linker may have the appropriate length to reach the catalytic site.

Improving potency by targeting the catalytic site

Based on the above results, we hypothesized that the inhibitory potency toward Cif could be improved by connecting the lead compound to a moiety that directly interacts with catalytic residues. A series of compounds were designed to target the catalytic site by extending the R_4 position. As shown in Scheme 2, these compounds were synthesized by Suzuki-Miyaura cross coupling between an iododiphenyl ether **7** and various substituted phenylboronic acids or esters, using $Pd(PPh_3)_4$ as a palladium catalyst and sodium carbonate as a base.[18] Their potencies as Cif inhibitors are shown in Table 3.

A compound with *para* carboxylic acid (**8b**) showed a significant loss of activity, while compounds with *para* amide (**8c**), urea (**8h**), or ketone (**8j**) showed potencies almost 10-fold higher than that of the lead compound, reaching the theoretical limit of quantification (half of the enzyme concentration) of our fluorescent-based Cif inhibition assay ([E]=0.6 μM in the assay). For more classical epoxide hydrolases, ureas and amides are pharmacophores for potent inhibitors that establish bonds with catalytic residues, but ketones are not,[16b] underscoring the distinct chemistry of the Cif active site. In the case of free amides, both *para* (**8c**) and *meta* (**8d**) substituents yielded high potencies, with the *para* substituent slightly favored. In the case of nitrile, the *meta* substituent (**8f**) showed higher potency but the *para* substituent (**8e**) showed significant decrease in potency. Compounds with a methyl amide (**8g**) or a sulfonamide substituent (**8k**) also showed significantly lower potency than corresponding free amide.

Surface plasmon resonance (SPR)

To confirm potency, particularly for our highest-affinity compounds, binding interactions between Cif and inhibitors were further examined by surface plasmon resonance (SPR). Results are shown in Table S5 and Figure S6. Compound **1a** and tiratricol showed similar affinity (K_D), and compounds **8c**, **8h** and **8j** showed 30- to 50-fold higher affinity than lead compound **1a**. Overall, the affinity values from the SPR experiments were approximately 10- to 40-fold weaker than the IC_{50} values obtained from the enzyme activity-based assay. Discrepancies between SPR and solution phase experiments have been reported in several protein-ligand interaction analyses[19], and may be due to conformational change by immobilization on the chip surface, cooperative effects, or differences in experimental conditions, such as the presence of surfactant and DMSO concentration in the running buffer. Identification of the cause of this discrepancy is the subject of further research. The dissociation rate constants (k_d; Table S5) suggest that **8c**, **8h** and **8j** have residence times between 2 and 4 seconds. This is much shorter than the best inhibitors for the human soluble epoxide hydrolase (sEH)[20], suggesting that further optimization of Cif inhibitors is possible.

Structures of second-generation Cif inhibitors

To further characterize the interaction between the new inhibitors and the Cif protein, we pursued a co-crystallization strategy and determined structures of the resulting complexes by X-ray diffraction. As shown in Figures 3A and 3B, the amide or urea moieties in compounds **8c** (purple) and **8h** (blue) interact with catalytic residues: the nucleophile Asp129, and Tyr239 and His177, which coordinate with the epoxide substrate.[5a] The NH group of amide and urea forms hydrogen bonds with Asp129, while the oxygen in the carbonyl forms hydrogen bonds to His177 and Tyr239. As with the acetate in the Cif:**1a** structure, the binding of **8c** and **8h** occupies the volume and thus replaces the tetrahedral water network found in the apo crystal structure (Figure 2D, cyan). By shifting the specific hydrogen-bonding network in the active site, **8c** and **8h** promote a hydrogen bond between His297 and Asp129. This new bond displaces the hydrogen bond with the catalytic water that is activated by the His297/Glu153 pair under hydrolysis conditions.

The structures also provide a framework to interpret the structure-activity relationship of Cif inhibitors targeting the catalytic site (Table 3, Table S5). It appears that the *meta* substituents (**8d** and **8f**) can each be accommodated at the edge of the catalytic core. Interestingly, among the *para* substituents either an amide (**8c**), a urea (**8h**) or a ketone (**8j**) moiety causes a substantial increase in potency against Cif. Although chemically distinct, each of these groups can be sterically accommodated between the catalytic aspartic acid and the ring-opening pair, forming hydrogen bonds that lie roughly within the plane of view defined by Figure 3. In contrast, weaker binding affinities are observed for *para* substituents with charge incompatibility (**8b**), out-of-plane hydrogen-bond orientations (**8k**), or a combination of steric and hydrogen-bonding incompatibility (**8e**, **8g**, **8i**).

Selectivity profile and *in vitro* metabolic stability of selected compounds

Three inhibitors, **8c**, **8h** and **8j**, were selected based on their Cif inhibitory potency (Table 3). Thyroid receptor induction activity (relative to 10 nM T_3) was measured at a concentration of 10 μM. Results (Table 4) showed that compounds **8c**, **8h** and **8j** lost their thyroid hormone agonistic activity (EC_{50}>10 μM), while they displayed a weak antagonistic activity (Table 4, Tables S6 & S7). Globally, compared to **1a**, the novel Cif inhibitors are more than 150,000-fold more selective for Cif than for the thyroid hormone receptor. Next, inhibition of human sEH and microsomal epoxide hydrolase (mEH) was measured. The IC_{50} values obtained ($\approx$ 8 μM for sEH, and 20-100 μM for mEH) are 100-10,000 fold higher than the best inhibitors for these enzymes[16b], suggesting that **8c**, **8h** and **8j** are poor inhibitors for the mammalian EHs. Given the potency of these compounds against Cif, they have at least a 27-fold selectivity toward Cif over sEH and at least a 50-fold selectivity toward Cif over mEH.

Metabolic stability of the three selected compounds was then studied in both liver microsomes and cell cultures.[21] Results (Table 4) indicate that compound **8h** is the most stable of the trio, followed in order by **8c** and **8j**. Compound **8a**, which does not have a substituent on the biphenyl ring (Table 3), had a half-life longer than 60 minutes in the human liver microsomal stability assay (63% remained after 60 min incubation). This value is more than double the corresponding value for **8h**, suggesting that the substituent on the

biphenyl ring is the most susceptible to metabolism. It should be noted that phenolic moieties are subject to phase II metabolic processes such as glucuronidation and sulfation[22], which could increase the clearance and thus decrease the bioavailability of these compounds *in vivo.*

Finally, we investigated the physico-chemical properties of the selected compounds. While the three compounds have similar molecular weight, compound **8h** has a lower melting point. In addition, this compound has a lower predicted LogP and much higher aqueous solubility, without DMSO as a co-solvent, than **8c** and **8j**, suggesting that **8h** should be easier to formulate, and should be more bioavailable. As expected from their lipophilicity, these compounds showed high plasma protein binding, which may limit their target accessibility and thus hamper their efficacy *in vivo.* It should be noted, however, that plasma protein binding could also help drug solubilization and distribution in the body.[23] Note that the reported Cif IC_{50} values were determined in the presence of high BSA concentration (0.1 mg/mL) to make the assay more representative of *in vivo* conditions. In terms of toxicity *in vitro*, neither **8c** nor **8h** showed cytotoxicity when applied to GH3.TRE-Luc cells or polarized monolayers of airway epithelial cells at concentrations up to 10 μM (Figures S7 & S8). Overall, in terms of potency, selectivity, metabolic stability, solubility and toxicity, compound **8h** is the most suitable for further *in vitro* and *in vivo* experiments to determine efficacy of Cif inhibitors against *Pseudomonas* infection.

CONCLUSION

Here we describe a series of potent and selective Cif inhibitors, rationally designed by combining insights from classical medicinal chemistry and crystallographic analysis of Cif:lead binding interactions. Compounds synthesized using this strategy show an approximately 10-fold increase in inhibitory potency toward the primary target, and also a more than 15,000-fold decrease in the critical off-target potency toward thyroid hormone receptor. The binding of these second-generation inhibitors was further analyzed by SPR and X-ray crystallography.

Given their *in vitro* stability and physico-chemical properties (Table 4), these inhibitors may have a short half-life, low bioavailability, and low accessibility to the target enzyme *in vivo.* Nevertheless, because of their increased potency against Cif and lack of thyroid hormone-like activity (Table 4), these new inhibitors will be useful in the study of the mechanisms of Cif virulence, as well as determining the *in vivo* functions of Cif and the efficacy of Cif inhibitors against *Pseudomonas* infection. Cif prevents deubiquitination of CFTR by ubiquitin specific peptidase 10.[24] To our knowledge, there are no reports of endogenous epoxides or diols that regulate the ubiquitin/proteasome system. An approach combining inhibitors and metabolomics should help identify the endogenous substrates of Cif.[25] These inhibitors are not only improved Cif inhibitors, but also represent potential inhibitors of bacterial EHs with similar active-site geometries.

EXPERIMENTAL SECTION

General

All reagents and solvents were purchased from commercial suppliers and were used without further purification. Compound **1a** was purchased from Cayman Chemicals (Purity 98%). All reactions were performed in an inert atmosphere of dry nitrogen or argon. Melting points were determined using an OptiMelt melting point apparatus. ^{1}H and ^{13}C NMR spectra were collected using a Varian 600, 400 or 300 MHz spectrometer with chemical shifts reported relative to residual deuterated solvent peaks or a tetramethylsilane internal standard. Accurate masses were measured using an LTQ orbitrap hybrid mass spectrometer (HRMS) or Micromass LCT ESI-TOF-MS (ESI-TOF-MS). The purity of the compounds that were tested in the assay was determined by reverse phase HPLC-DAD and found to be > 95% based on monitoring absorption at 254 nm. Reactions were monitored on TLC plates (silica gel matrix, fluorescent indicator, Sigma-Aldrich, 99569), and spots were either monitored under UV light (254 mm) or stained with phosphomolybdic acid. The same TLC system was used to test purity, and all final products showed a single spot on TLC with both phosphomolybdic acid and UV absorbance, and when measured gave a sharp melting point for crystalline compounds. FT-IR spectra were recorded on a Thermo Scientific NICOLET IR100 FT-IR Spectrometer. The elemental analysis was conducted by Midwest Microlab, Indianapolis, IN. Compound **1a** analogs were synthesized using methods similar to the one previously described for thyroid hormone analogs.[11] Chemical characterization of representative compounds is described below, and others are included in detailed synthetic methods in Supporting Information.

General procedure A: S$_N$Ar

To an ice-cold DMF solution of phenol **2** (1.1 equiv) was slowly added 1 M NaOH$_{aq}$ (1.1 equiv), followed by compound **3** (1.0 equiv) in DMF. The reaction was slowly warmed up to rt, and stirred for 1-24 h. To this solution was added water. The mixture was extracted with hexane/ethyl acetate (5:1) mixture three times. The organic layer was combined, washed with brine, dried over MgSO$_4$, filtered and concentrated *in vacuo*.

1,3-Dibromo-2-(3-isopropyl-4-methoxyphenoxy)-5-nitrobenzene (4a)—

Compound **4a** was synthesized from *3-isopropyl-4-methoxyphenol* (**2a**) and *1, 3-dibromo-2-iodo-5-nitrobenzene* (**3a**) to give the desired product (1.85 g, 85 %) as a yellow powder. ^{1}H NMR (600 MHz, CDCl$_3$) δ 8.50 (s, 2H, H-7, H-9), 6.81 (d, *J* = 3.5 Hz, 1H, H-1), 6.71 (d, *J* = 9.2 Hz, 1H, H-4), 6.43 (dd, *J* = 8.9, 3.5 Hz, 1H, H-5), 3.79 (s, 3H, C*H$_3$*O), 3.30 – 3.28 (m, 1H, isopropyl C*H*), 1.18 (d, *J* = 6.9 Hz, 6H, isopropyl (C*H$_3$*)$_2$). ^{13}C NMR (151 MHz, CDCl$_3$) δ 155.5, 152.9, 150.0, 145.0, 139.3, 128.5, 119.5, 114.4, 111.9, 111.0, 55.9, 27.1, 22.6.

General procedure B: Deprotection of methoxy moiety

To an ice-cold DCM solution of diphenylether **4**, a 1 M boron tribromide (1.2 equiv) solution in DCM was added dropwise. The reaction was slowly warmed up to rt, and stirred for 1-24 h. To this solution was slowly added methanol at 0 °C, then warmed to rt. The solution was washed with saturated NaHCO$_3$ aqueous solution, and the aqueous layer was

extracted with DCM three times. The organic layer was combined and washed with brine, dried over $MgSO_4$, filtered and concentrated *in vacuo*.

4-(2, 6-Dibromo-4-nitrophenoxy)-2-isopropylphenol (5a)—Compound **5a** was synthesized from **4a** to give the desired product (1.9 g, quant) as a yellow powder; mp 106-107 °C; ^{1}H NMR (600 MHz, $CDCl_3$) δ 8.50 (s, 2H, H-7, H-9), 6.79 (d, *J* = 3.1 Hz, 1H, H-1), 6.65 (d, *J* = 8.7 Hz, 1H, H-4), 6.39 (dd, *J* = 8.7, 3.1 Hz, 1H, H-5), 4.54 (s, 1H, O*H*), 3.18 (septet, *J* = 6.9 Hz, 1H, isopropyl C*H*), 1.23 (d, *J* = 6.9 Hz, 6H, isopropyl (C*H3*)2). ^{13}C NMR (151 MHz, $CDCl_3$) δ 155.5, 150.2, 148.8, 145.0, 136.7, 128.6, 119.4, 116.0, 114.4, 112.6, 27.5, 22.5. ESI-TOF-MS (+) calcd for $C_{15}H_{14}Br_2NO_4$ (M+H)[+] 429.92, found 429.89. Purity (HPLC-UV): 95% (*t*R=13.0 min).

General procedure C: Reduction of nitro moiety to a primary amine

To a THF solution of compound **5** (1.0 equiv) was added an aqueous solution of sodium dithionite (3.8 equiv) at rt, then the solution was heated to 50 °C and stirred 1-24 h. After cooling to rt, aqueous 1 M HCl was added and then the solution was neutralized by a solution of saturated $NaHCO_3$. The organic layer was separated, and the aqueous layer was extracted with ethyl acetate. The organic layer was combined and washed with brine, dried over $MgSO_4$, filtered and concentrated *in vacuo*.

4-(4-Amino-2, 6-dibromophenoxy)-2-isopropylphenol (6a)—Compound **6a** was synthesized from **5a** to give the desired product (1.38 g, 87%) as yellowish crystals; mp 186-187°C; ^{1}H NMR (600 MHz, DMSO-*d6*) δ 8.93 (s, 1H, O*H*), 6.87 (s, 2H, H-7, H-9), 6.64 (d, *J* = 8.7 Hz, 1H, H-4), 6.60 (d, *J* = 3.1 Hz, 1H, H-1), 6.25 (dd, *J* = 8.7, 3.1 Hz, 1H, H-5), 5.53 (s, 2H, N*H2*), 3.14 (septet, *J* = 6.9 Hz, 1H, isopropyl C*H*), 1.10 (d, *J* = 6.9 Hz, 6H, isopropyl (C*H3*)2). ^{13}C NMR (151 MHz, DMSO-*d6*) δ 150.1, 149.1, 148.2, 137.8, 135.3, 118.0, 117.0, 115.2, 112.6, 111.3, 26.5, 22.4. ESI-TOF-MS (+) calcd for $C_{15}H_{16}Br_2NO_2$ (M+H)[+] 399.95, found 399.94. Purity (HPLC-UV): 99% (*t*R=10.9 min).

General procedure D: Amide bond formation

To an ice-cold MTBE solution of aniline **6** (1.0 equiv) was added a solution of saturated $NaHCO_3$ or 1 M NaOH, followed by slowly adding the corresponding acid chloride (1.1 equiv). This solution was stirred at rt 1-24 h, then 1 M HCl aqueous solution was added. The reaction mixture was extracted with ethyl acetate. The organic layer was combined and washed with 1 M HCl_{aq} twice, saturated aqueous $NaHCO_3$ solution 4 times, and brine, dried over $MgSO_4$, filtered and concentrated *in vacuo*. The target compound was purified by column chromatography, and further purified by recrystallization from acetone/DCM/hexane when possible.

N-(3, 5-Dibromo-4-(4-hydroxy-3-isopropylphenoxy) phenyl) acetamide (1b)—Compound **1b** was synthesized from **6a** and acetyl chloride to give the desired product (99 mg, 56%) as a white powder; mp 172-173 °C; ^{1}H NMR (600 MHz, DMSO-*d6*) δ 10.24 (s, 1H, N*H*), 9.02 (s, 1H, O*H*), 7.96 (s, 2H, H-7, H-9), 6.67 – 6.64 (m, 2H, H-1, H-4), 6.26 (dd, *J* = 9.4, 2.2 Hz, 1H, H-5), 3.16 – 3.14 (m, 1H, isopropyl C*H*), 2.07 (s, 3H, COC*H3*), 1.11 (d, *J* = 7.0 Hz, 6H, isopropyl (C*H3*)2). ^{13}C NMR (151 MHz, DMSO-*d6*) δ 168.8, 149.5, 149.3,

143.8, 138.2, 135.6, 122.7, 117.8, 115.3, 112.8, 111.4, 26.5, 24.0, 22.3. ESI-TOF-MS (−) calcd for $C_{17}H_{16}Br_2NO_3$ (M-H)$^-$ calcd 439.96 found 439.97. Purity (HPLC-UV): 98% (^tR=10.8 min).

General procedure E: Suzuki-Miyaura coupling

To a DME solution of compound **7** (80 mg, 177 μmol, 1.0 equiv) were added Pd(PPh$_3$)$_4$ (10 mg, 8.7 μmol, 0.05 equiv), an aqueous solution of Na$_2$CO$_3$ (400 mg in 1 mL H$_2$O), and corresponding boronic acid or boronate ester (212 μmol, 1.2 equiv) in 1 mL ethanol. This solution was stirred at 71 °C overnight. After cooling to rt, ethyl acetate and 1 M HCl$_{aq}$ were added and extracted 4 times with ethyl acetate. The organic layer was combined and washed with brine, dried over MgSO$_4$, filtered and concentrated *in vacuo*. The target compound was purified by column chromatography, and recrystallized from acetone/DCM/hexane.

5′-(2,6-Dichloro-4-propionamidophenoxy)-2′-hydroxy-[1,1′-biphenyl]-4-carboxamide (8c)—Compound **8c** was synthesized from compound **7** and 4-aminocarbonylphenylboronic acid. The product was obtained as an off-white powder (14 mg, 18%); TLC R_F=0.4 (DCM:MeOH=30:1); mp 261.3–262.0 °C; IR (neat) 3339 (broad), 1648, 1592, 1532, 1531, 1462 cm^{-1}; ^{1}H NMR (600 MHz, DMSO-d_6) δ 10.22 (s, 1H, N*H*), 9.48 (s, 1H, O*H*), 7.96 (s, 1H, NH*H*), 7.88 – 7.83 (m, 2H, biphenyl-*H$_2$*), 7.82 (s, 2H, H-7, H-9), 7.57 – 7.55 (m, 2H, biphenyl-*H$_2$*), 7.34 (s, 1H, NH*H*), 6.90 (d, *J* = 8.8 Hz, 1H, H-4), 6.75 (d, *J* = 3.1 Hz, 1H, H-1), 6.64 (dd, *J* = 8.8, 3.2 Hz, 1H, H-5), 2.34 (q, *J* = 7.5 Hz, 2H, C*H$_2$*), 1.09 (t, *J* = 7.5 Hz, 3H, C*H$_3$*). ^{13}C NMR (151 MHz, DMSO-d_6) δ 172.6, 167.7, 149.7, 149.6, 141.5, 140.6, 137.7, 132.6, 128.7, 128.6, 127.6, 127.2, 119.1, 117.1, 116.0, 114.8, 30.7, 9.4. HRMS (+) calcd for $C_{22}H_{19}Cl_2N_2O_4^+$ (M+H) 445.0716. Found 445.0717. Purity (HPLC-UV): 99% (^tR=9.2 min). Anal. C 59.09, H 4.14, N 6.13%, calcd for $C_{22}H_{18}Cl_2N_2O_4$, C 59.34, H 4.07, N 6.29%.

Cif preparation

Recombinant Cif-His was prepared as described previously.[5b, 26] Stocks of purified proteins were stored at 4 °C until used. Since esterase and glutathione transferases can give a high background fluorescence when using cyano (6-methoxy-naphthalen-2-yl) methyl glycidyl carbonate (CMNGC) as Cif substrate, it is important to evaluate the purity of Cif for the absence of these and of similar biochemicals. The purified enzyme was tested for contamination with esterase activity and glutathione transferase activity as previously described[27].

Fluorescent-based Cif inhibitory assay

IC$_{50}$ values were determined using a sensitive fluorescent-based assay similar to the method previously described for other EHs.[5b, 28] Cyano (6-methoxy-naphthalen-2-yl) methyl glycidyl carbonate (CMNGC) was used as a fluorescent reporter substrate. Recombinant Cif (0.6 μM) was incubated with inhibitors for 5 min in sodium phosphate buffer (20 mM pH 7.0) containing 50 mM NaCl and 0.1 mg/mL of BSA at 37 °C prior to substrate introduction ([S] = 25 μM).

Activity was measured by determining the appearance of the 6-methoxy-2-naphthaldehyde with an excitation wavelength of 330 nm and an emission wavelength of 465 nm for 10 min. Reported IC_{50} values are the average of triplicates with at least two datum points above and at least two below the IC_{50}. The fluorescent-based assay as performed here has a standard error between 10% and 20%, suggesting that differences of two-fold or greater are significant. Control experiments without Cif (inhibitor and substrate) were used to evaluate the intrinsic fluorescence of inhibitors. For compounds showing $IC_{50}>50$ μM (compounds **1g**, **1h**, and **1k**), solubility under assay conditions was measured using a method described previously[29]. Compounds **1g** and **1k** showed solubility 50<S<100 μM, while compound **1h** showed 25<S<50 μM.

Surface plasmon resonance

The interactions between Cif and inhibitors were analyzed by surface plasmon resonance using a BIAcore T100. The running buffer for immobilization was HBS-P (pH 7.4), which contains 10 mM HEPES, 150 mM NaCl, and 0.05% (*v/v*) Tween 20 surfactant. Cif was coupled to the surface of a CM5 sensor chip using standard amine-coupling chemistry with a 7 min injection of Cif (15 μg/mL) diluted in 10 mM sodium acetate (pH 4.5). Cif protein was immobilized at 4000-5000 RU. Remaining activated groups were blocked with a 7 min injection of 1 M ethanolamine HCl (pH 8.5). Binding assays were performed at 37 °C at a flow rate of 30 μL/min with a 40 sec injection of inhibitors followed by washing with buffer for 40 sec. Sodium phosphate buffer (20 mM pH 7.0) containing 50 mM NaCl and 0.05% (*v/v*) Tween 20 with 4% (*v/v*) DMSO was used as a running buffer in the assay. The measured signals were double-referenced from reference curves generated by an uncoated flow cell and several injections of running buffer. Experimental data were analyzed using BIAevaluation 1.0 software (BIAcore).

X-ray structure analysis

Cif:inhibitor co-crystals were obtained by vapor diffusion against 400 μL of reservoir solution in a 4 μL hanging drop at 291 K.[5a, 30] A solution of 5 mg/mL Cif protein containing 200 μM inhibitor was mixed in a 1:1 ratio with reservoir solution consisting of 12-16% (*w/v*) polyethylene glycol 8000, 125 mM $CaCl_2$, 100 mM sodium acetate (pH 5), 200 μM inhibitor, and 0.2% (*v/v*) DMSO. Prior to data collection, crystals were washed in cryoprotectant solution consisting of 12-16% (*w/v*) polyethylene glycol 8000, 125 mM $CaCl_2$, 100 mM sodium acetate (pH 5), 200 μM inhibitor, 0.2% (*v/v*) DMSO, and 20% (*w/v*) glycerol and flash cooled by plunging into a liquid nitrogen bath. Oscillation data were collected at 100 K at the X6A beamline of the National Synchrotron Light Source at Brookhaven National Laboratory (PDB ID 5HKB) and the 5.0.1 beamline of the Advance Light Source at Lawrence Berkeley National Laboratory (PDB IDs 5HKA, 5HK9). Diffraction images were processed and scaled with the XDS package (v January 10, 2014).[31] Molecular replacement using apo-Cif-WT as the search model (PDB ID 3KD2) revealed two dimers in the asymmetric unit. Iterative rounds of automated refinement were carried out with Phenix (v 1.7.33928).[32] WinCoot (v 0.7)[33] was used for manual adjustment of the model, and PyMOL (v 1.3)[34] was used to render structure images of the final models of chain B, in which the active-site structures are best defined. Structure figures were assembled in Adobe Illustrator CS6 (v16.0.4).

Thyroid hormone activity assay

Thyroid hormone activity was measured by the assay described previously with slight modifications.[14] GH3.TRE-Luc cells were seeded at 80% confluency in 75 cm^2 culture flasks (Corning, Schiphol-Rijk, Netherlands) in regular growth medium. Cells were collected and seeded into 24-well plates for an additional period of 24 h, and incubated for 24 h in the presence or absence of T$_3$, with the indicated test chemical in DMSO. The DMSO concentration in 500 μL of exposure medium was always the same for all exposures within an experiment and always kept 0.5% (*v/v*) to avoid cytotoxicity. Cell viability in each well was determined by measuring total protein concentration using the bicinchoninic acid (BCA) assay following the manufacturer's protocol. Luciferase activity was measured on lysed cells on an Infinite M1000 plate reader (Tecan Group AG, Zürich, Switzerland).

Supplementary Material

Refer to Web version on PubMed Central for supplementary material.

ACKNOWLEDGEMENTS

ABBREVIATIONS USED

CFTR	cystic fibrosis transmembrane conductance regulator
Cif	CFTR inhibitory factor
EH	epoxide hydrolase
T$_3$	triiodothyronine
sEH	soluble epoxide hydrolase
mEH	microsomal epoxide hydrolase
CMNGC	cyano (6-methoxy-naphthalen-2-yl) methyl glycidyl carbonate
***t*-DPPO**	[^{3}H] *trans*-diphenylpropene oxide
TR	thyroid hormone receptor
SPR	surface plasmon resonance

REFERENCES

1. a Dudley MN, Loutit J, Griffith DC. Aerosol antibiotics: Considerations in pharmacological and clinical evaluation. Curr. Opin. Biotechnol. 2008; 19(6):637–643. [PubMed: 19036576] b Davies JC, Bilton D. Bugs, biofilms, and resistance in cystic fibrosis. Respir. Care. 2009; 54(5):628–640. [PubMed: 19393107]

2. Mah T-F, Pitts B, Pellock B, Walker GC, Stewart PS, O'Toole GA. A genetic basis for Pseudomonas aeruginosa biofilm antibiotic resistance. Nature. 2003; 426(6964):306–310. [PubMed: 14628055]

3. a Cohen TS, Prince A. Cystic fibrosis: A mucosal immunodeficiency syndrome. Nat. Med. 2012; 18(4):509–519. [PubMed: 22481418] b Stanton BA, Coutermarsh B, Barnaby R, Hogan D. Pseudomonas aeruginosa reduces VX-809 stimulated F508del-CFTR chloride secretion by airway epithelial cells. PLoS One. 2015; 10(5):e0127742. [PubMed: 26018799] c Jolly AL, Takawira D, Oke OO, Whiteside SA, Chang SW, Wen ER, Quach K, Evans DJ, Fleiszig SMJ. Pseudomonas aeruginosa-induced bleb-niche formation in epithelial cells is independent of actinomyosin contraction and enhanced by loss of cystic fibrosis transmembrane-conductance regulator osmoregulatory function. mBio. 2015; 6(2)d Trinh NTN, Bilodeau C, Maillé É, Ruffin M, Quintal M-C, Desrosiers M-Y, Rousseau S, Brochiero E. Deleterious impact of Pseudomonas aeruginosa on cystic fibrosis transmembrane conductance regulator function and rescue in airway epithelial cells. Eur. Respir. J. 2015; 45(6):1590–1602. [PubMed: 25792634] e Rubino R, Bezzerri V, Favia M, Facchini M, Tebon M, Singh A, Riederer B, Seidler U, Iannucci A, Bragonzi A, Cabrini G, Reshkin S, Tamanini A. Pseudomonas aeruginosa reduces the expression of CFTR via post-translational modification of NHERF1. Pflugers Arch. / Eur. J. Physiol. 2014; 466(12):2269–2278. [PubMed: 24595473]

4. Ballok AE, O'Toole GA. Pouring salt on a wound: Pseudomonas aeruginosa virulence factors alter Na+ and Cl– flux in the lung. J. Bacteriol. 2013; 195(18):4013–4019. [PubMed: 23836869]

5. a Bahl CD, Morisseau C, Bomberger JM, Stanton BA, Hammock BD, O'Toole GA, Madden DR. Crystal structure of the cystic fibrosis transmembrane conductance regulator inhibitory factor Cif reveals novel active-site features of an epoxide hydrolase virulence factor. J. Bacteriol. 2010; 192(7):1785–1795. [PubMed: 20118260] b Bahl CD, Hvorecny KL, Bomberger JM, Stanton BA, Hammock BD, Morisseau C, Madden DR. Inhibiting an epoxide hydrolase virulence factor from Pseudomonas aeruginosa protects CFTR. Angew. Chem. Int. Ed. 2015; 54(34):9881–9885.c Bahl DD, Madden DR. Pseudomonas aeruginosa Cif defines a distinct class of α/β epoxide hydrolases utilizing a His/Tyr ring-opening pair. Protein Pept. Lett. 2012; 19(2):186–193. [PubMed: 21933119]

6. Evans RW, Braverman LE. Use of 125I-triiodothyroacetic acid to measure nuclear thyroid hormone receptor. Endocr. Res. 1986; 12(1):37–47. [PubMed: 3009172]

7. a Ma RCW, Chan MHM, Poon WT, So WY, Chow CC. Thyroid dysfunction due to over-the-counter usage of tiratricol. Intern. Med. J. 2008; 38(7):611–612. [PubMed: 18715309] b Cohen-Lehman J, Charitou MM, Klein I. Tiratricol-induced periodic paralysis: a review of nutraceuticals affecting thyroid function. Endocr. Pract. 2011; 17(4):610–615. [PubMed: 21803722] c Marks D. Dangers of OTC herbal supplements: Dilated cardiomyopathy after ingestion of TRIAC (triiodothyroacetic acid, Tiratricol). Internet J. Endocrinol. 2006; 3(2)

8. Singh L, Pressly B, Mengeling BJ, Fettinger JC, Furlow JD, Lein PJ, Wulff H, Singh V. Chasing the elusive benzofuran impurity of the THR antagonist NH-3: Synthesis, isotope labeling, and biological activity. J. Org. Chem. 2016; 81(5):1870–1876. [PubMed: 26849160]

9. Berkenstam A, Kristensen J, Mellström K, Carlsson B, Malm J, Rehnmark S, Garg N, Andersson CM, Rudling M, Sjöberg F, Angelin B, Baxter JD. The thyroid hormone mimetic compound KB2115 lowers plasma LDL cholesterol and stimulates bile acid synthesis without cardiac effects in humans. Proc. Natl. Acad. Sci. USA. 2008; 105(2):663–667. [PubMed: 18160532]

10. a Joharapurkar AA, Dhote VV, Jain MR. Selective thyromimetics using receptor and tissue selectivity approaches: Prospects for dyslipidemia. J. Med. Chem. 2012; 55(12):5649–5675. [PubMed: 22512468] b Baxter JD, Webb P. Thyroid hormone mimetics: potential applications in atherosclerosis, obesity and type 2 diabetes. Nat. Rev. Drug discov. 2009; 8(4):308–320. [PubMed: 19337272]

11. Chidambaram, R.; Kant, J.; Weaver, RE., Jr.; Yu, J.; Ghosh, A. Process for the preparation of aniline-derived thyroid receptor ligands with improved safety and economy. May 15. 2003 WO03039456 (A2)

12. Wilcken R, Zimmermann MO, Lange A, Joerger AC, Boeckler FM. Principles and applications of halogen bonding in medicinal chemistry and chemical biology. J. Med. Chem. 2013; 56(4):1363–1388. [PubMed: 23145854]

13. a Sinnokrot MO, Sherrill CD. Substituent effects in π–π interactions: Sandwich and T-shaped configurations. J. Am. Chem. Soc. 2004; 126(24):7690–7697. [PubMed: 15198617] b Bissantz C, Kuhn B, Stahl M. A medicinal chemist's guide to molecular interactions. J. Med. Chem. 2010; 53(14):5061–5084. [PubMed: 20345171]

14. Freitas J, Cano P, Craig-Veit C, Goodson ML, Furlow DJ, Murk AJ. Detection of thyroid hormone receptor disruptors by a novel stable in vitro reporter gene assay. Toxicol. In Vitro. 2011; 25(1):257–266. [PubMed: 20732405]

15. a Decker M, Adamska M, Cronin A, Di Giallonardo F, Burgener J, Marowsky A, Falck JR, Morisseau C, Hammock BD, Gruzdev A, Zeldin DC, Arand M. EH3 (ABHD9): The first member of a new epoxide hydrolase family with high activity for fatty acid epoxides. J. Lipid Res. 2012; 53(10):2038–2045. [PubMed: 22798687] b Arand M, Wagner H, Oesch F. Asp, Asp, and His form the catalytic triad of rat soluble epoxide hydrolase. J. Biol. Chem. 1996; 271(8):4223–4229. [PubMed: 8626766] c Gomez GA, Morisseau C, Hammock BD, Christianson DW. Human soluble epoxide hydrolase: Structural basis of inhibition by 4-(3-cyclohexylureido)-carboxylic acids. Protein Sci. 2006; 15(1):58–64. [PubMed: 16322563]

16. a Amano Y, Yamaguchi T, Tanabe E. Structural insights into binding of inhibitors to soluble epoxide hydrolase gained by fragment screening and X-ray crystallography. Bioorg. Med. Chem. 2014; 22(8):2427–2434. [PubMed: 24656800] b Morisseau C, Goodrow MH, Dowdy D, Zheng J, Greene JF, Sanborn JR, Hammock BD. Potent urea and carbamate inhibitors of soluble epoxide hydrolases. Proc. Natl. Acad. Sci. U. S. A. 1999; 96(16):8849–8854. [PubMed: 10430859] c Morisseau C, Newman JW, Wheelock CE, Hill T III, Morin D, Buckpitt AR, Hammock BD. Development of metabolically stable inhibitors of mammalian microsomal epoxide hydrolase. Chem. Res. Toxicol.; 2008; 21(4):951–957.d Morisseau C, Newman JW, Dowdy DL, Goodrow MH, Hammock BD. Inhibition of microsomal epoxide hydrolases by ureas, amides, and amines. Chem. Res. Toxicol. 2001; 14(4):409–415. [PubMed: 11304129]

17. Bahl CD, Hvorecny KL, Morisseau C, Gerber SA, Madden DR. Visualizing the mechanism of epoxide hydrolysis by the bacterial virulence enzyme Cif. Biochemistry. 2016; 55(5):788–797. [PubMed: 26752215]

18. Miyaura N, Suzuki A. Palladium-catalyzed cross-coupling reactions of organoboron compounds. Chem. Rev. 1995; 95(7):2457–2483.

19. a Nieba L, Krebber A, Plückthun A. Competition BIAcore for measuring true affinities: Large differences from values determined from binding kinetics. Anal. Biochem. 1996; 234(2):155–165. [PubMed: 8714593] b Schuck P. Use of surface plasmon resonance to probe the equilibrium and dynamic aspects of interactions between biological macromolecules. Annu. Rev. Biophys. Biomol. Struct. 1997; 26(1):541–566. [PubMed: 9241429] c Cushing PR, Fellows A, Villone D, Boisguérin P, Madden DR. The relative binding affinities of PDZ partners for CFTR: A biochemical basis for efficient endocytic recycling. Biochemistry. 2008; 47(38):10084–10098. [PubMed: 18754678]

20. Lee KSS, Liu J-Y, Wagner KM, Pakhomova S, Dong H, Morisseau C, Fu SH, Yang J, Wang P, Ulu A, Mate CA, Nguyen LV, Hwang SH, Edin ML, Mara AA, Wulff H, Newcomer ME, Zeldin DC, Hammock BD. Optimized inhibitors of soluble epoxide hydrolase improve in vitro target residence time and in vivo efficacy. J. Med. Chem. 2014; 57(16):7016–7030. [PubMed: 25079952]

21. Kim IH, Nishi K, Kasagami T, Morisseau C, Liu J-Y, Tsai HJ, Hammock BD. Biologically active ester derivatives as potent inhibitors of the soluble epoxide hydrolase. Bioorg. Med. Chem. Lett. 2012; 22(18):5889–5892. [PubMed: 22901393]

22. Baojian W, Sumit B, Shengnan M, Xiaoqiang W, Ming H. Regioselective sulfation and glucuronidation of phenolics: Insights into the structural basis. Curr. Drug Metab. 2011; 12(9):900–916. [PubMed: 21933112]

23. Smith DA, Di L, Kerns EH. The effect of plasma protein binding on in vivo efficacy: Misconceptions in drug discovery. Nat. Rev. Drug discov. 2010; 9(12):929–939. [PubMed: 21119731]

24. Bomberger JM, Ye S, MacEachran DP, Koeppen K, Barnaby RL, O'Toole GA, Stanton BA. A Pseudomonas aeruginosa toxin that hijacks the host ubiquitin proteolytic system. PLoS Path. 2011; 7(3):e1001325.

25. Prosser GA, Larrouy-Maumus G, de Carvalho LPS. Metabolomic strategies for the identification of new enzyme functions and metabolic pathways. EMBO rep. 2014; 15(6):657–669. [PubMed: 24829223]

26. MacEachran DP, Ye S, Bomberger JM, Hogan DA, Swiatecka-Urban A, Stanton BA, O'Toole GA. The Pseudomonas aeruginosa secreted protein PA2934 decreases apical membrane expression of the cystic fibrosis transmembrane conductance regulator. Infect. Immun. 2007; 75(8):3902–3912. [PubMed: 17502391]

27. Morisseau C, Merzlikin O, Lin A, He G, Isela Padilla WF, Denison MS, Pessah IN, Hammock BD. Toxicology in the fast lane: Application of high-throughput bioassays to detect modulation of key enzymes and receptors. Environ. Health Perspect. 2009; 117(12):1867–1872. [PubMed: 20049205]

28. a Morisseau C, Bernay M, Escaich A, Sanborn JR, Lango J, Hammock BD. Development of fluorescent substrates for microsomal epoxide hydrolase and application to inhibition studies. Anal. Biochem. 2011; 414(1):154–162. [PubMed: 21371418] b Jones PD, Wolf NM, Morisseau C, Whetstone P, Hock B, Hammock BD. Fluorescent substrates for soluble epoxide hydrolase and application to inhibition studies. Anal. Biochem. 2005; 343(1):66–75. [PubMed: 15963942]

29. Morisseau C, Goodrow MH, Newman JW, Wheelock CE, Dowdy DL, Hammock BD. Structural refinement of inhibitors of urea-based soluble epoxide hydrolases. Biochem. Pharmacol. 2002; 63(9):1599–1608. [PubMed: 12007563]

30. Bahl CD, MacEachran DP, O'Toole GA, Madden DR. Purification, crystallization and preliminary X-ray diffraction analysis of Cif, a virulence factor secreted by Pseudomonas aeruginosa. Acta Crystallogr. 2010; F66(Pt 1):26–28.

31. Kabsch W. Automatic processing of rotation diffraction data from crystals of initially unknown symmetry and cell constants. J. Appl. Crystallogr. 1993; 26:795–800.

32. Adams PD, Afonine PV, Bunkoczi G, Chen VB, Davis IW, Echols N, Headd JJ, Hung L-W, Kapral GJ, Grosse-Kunstleve RW, McCoy AJ, Moriarty NW, Oeffner R, Read RJ, Richardson DC, Richardson JS, Terwilliger TC, Zwart PH. PHENIX: a comprehensive Python-based system for macromolecular structure solution. Acta Crystallogr. 2010; D66(2):213–221.

33. Emsley P, Cowtan K. Coot: Model-building tools for molecular graphics. Acta Crystallogr. 2004; D60(Pt 12 Pt 1):2126–2132.

34. DeLano, WL. The PyMOL molecular graphics system. DeLano Scientific LLC; Palo Alto, CA, USA: 2008. http://www.pymol.org

35. Ulu A, Appt S, Morisseau C, Hwang SH, Jones PD, Rose TE, Dong H, Lango J, Yang J, Tsai HJ, Miyabe C, Fortenbach C, Adams MR, Hammock BD. Pharmacokinetics and in vivo potency of soluble epoxide hydrolase inhibitors in cynomolgus monkeys. Br. J. Pharmacol. 2012; 165(5): 1401–1412. [PubMed: 21880036]
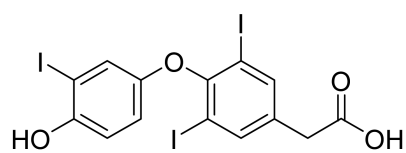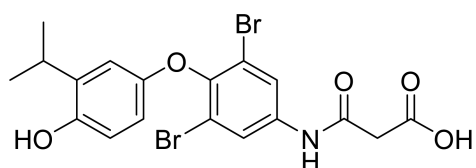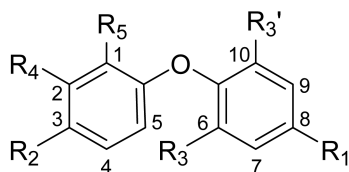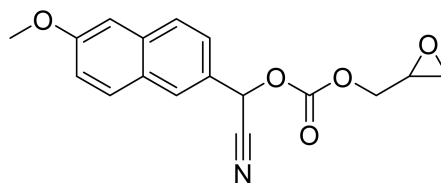
Figure 1.
Structures of lead compounds and their potency are shown while a general structure for Cif inhibitors and the substrate used for Cif assay are below.
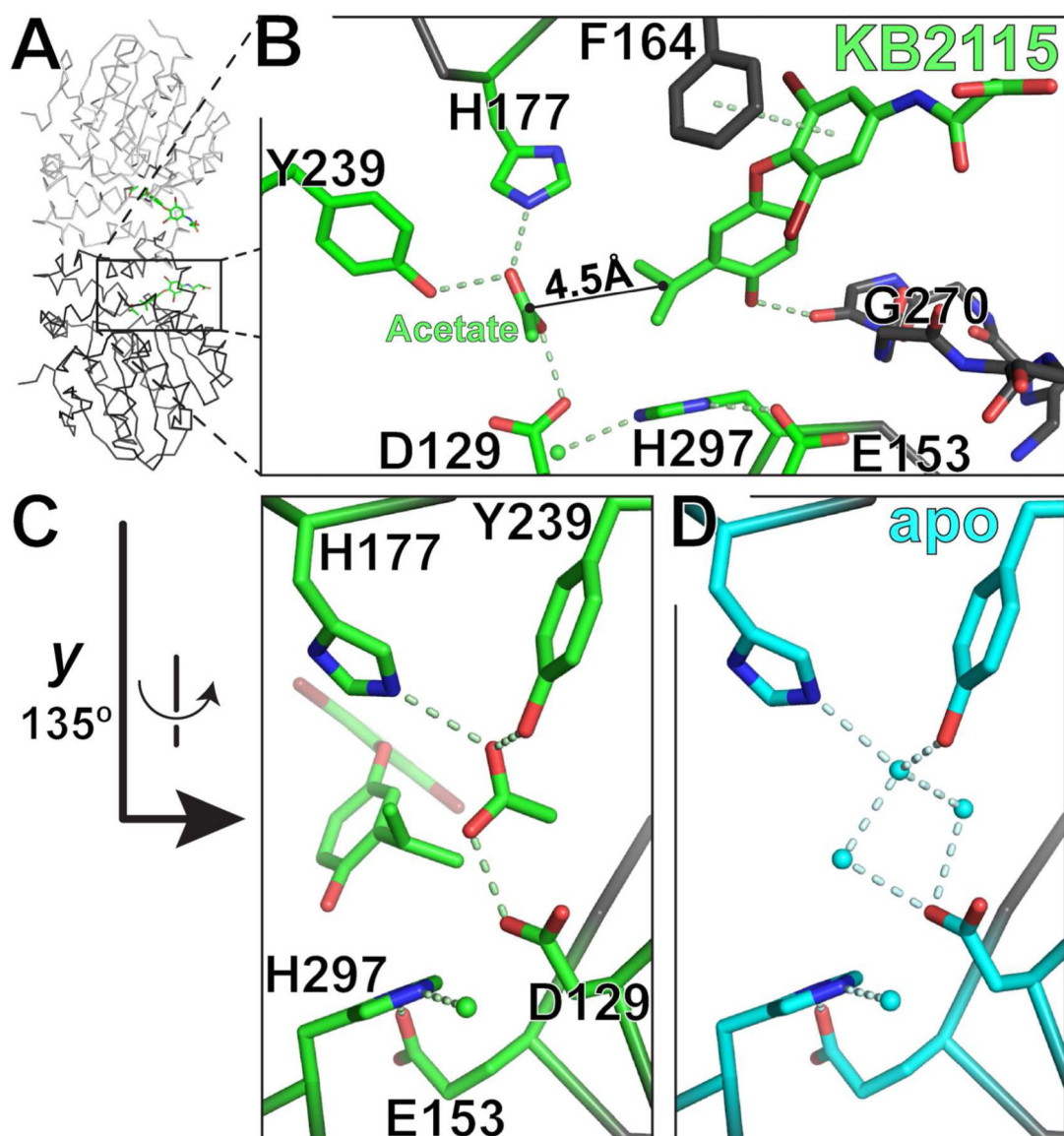
Figure 2.
X-ray crystal structure of lead compound **1a** in complex with Cif. (A) A C_{α}-trace shows the conformation of the Cif dimer, with active-site side chains and **1a** included as stick figures. (B) An expansion of the chain B inset highlighted in (A) displays the hydrogen bonding network and ring-stacking interaction (dashed lines) formed among **1a**, an acetate ion (green carbons), water molecules (green spheres), and active-site residues (carbons from catalytic residues in green; others in grey). Compound **1a** blocks entrance to the active site from the upper right. Potential bonds with halogens are shown in Figure S3. (C) The Cif active site rotated by roughly 135° highlights the hydrogen bonding network that connects Cif, **1a**, and a bound acetate ion. (D) The same view of apo Cif (cyan carbons and waters) shows the conserved positions of active-site side chains. Non-carbon atoms are colored by element (O, red; N, dark blue; Br, maroon).
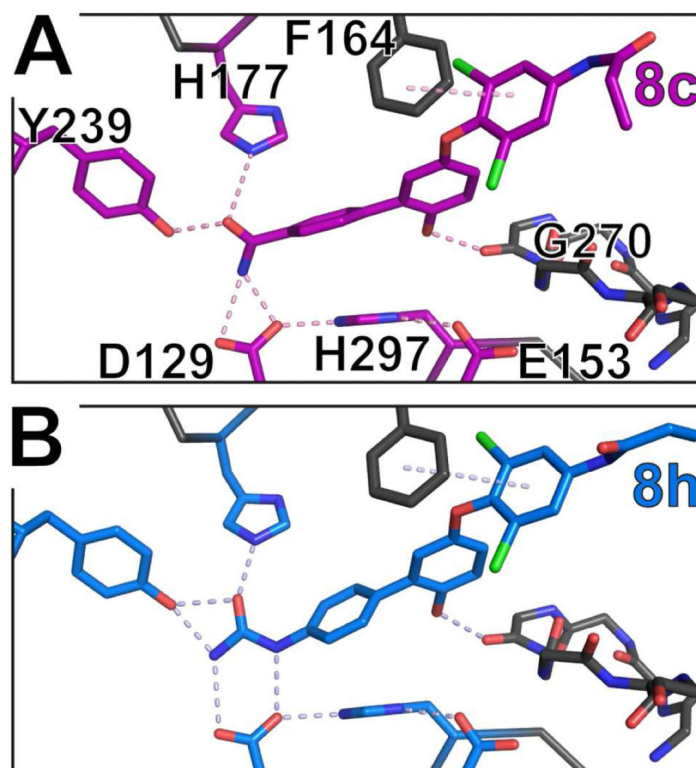
Figure 3.
X-ray structures of Cif:**8c** (A, purple carbons) and **8h** (B, blue carbons) complexes, with respective hydrogen bonding networks represented by dashed lines for chain B. Carbon atoms of catalytic and non-catalytic residues are shown in the same color as the corresponding ligand and in gray, respectively. Potential bonds with halogens are not shown. Non-carbon atoms are colored by element (O, red; N, dark blue; Cl, green).
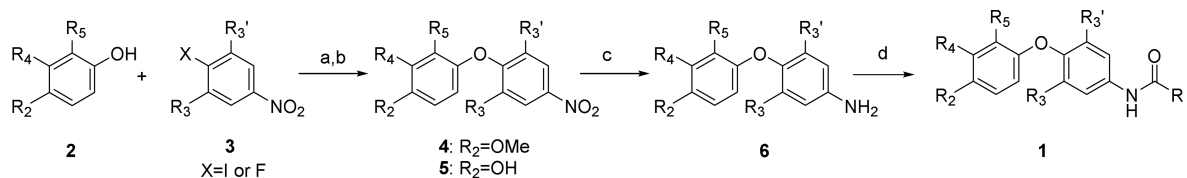
Reagents and conditions: (a) $NaOH_{aq}$, DMF (b) BBr_3, DCM (c) $Na_2S_2O_4$, THF/H_2O, 50 °C (d) R-COCl, MTBE, saturated $NaHCO_{3\ aq}$ or 1 M $NaOH_{aq}$.
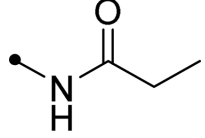
Scheme 1.
General synthetic scheme.
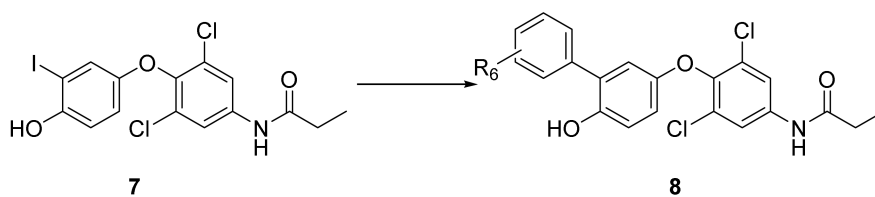
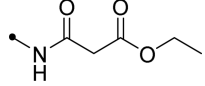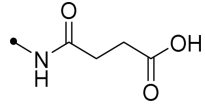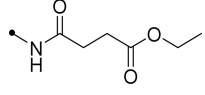Reagents and conditions: R_6-phenylboronic acid or ester, $Pd(PPh_3)_4$, Na_2CO_3, DME/EtOH/H_2O, 71°C.

**Scheme 2.**
Synthesis of compounds 8a-k by Suzuki-Miyaura coupling.

Table 1

Effect of R_1 moiety on Cif inhibitory potency
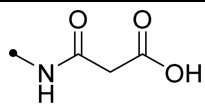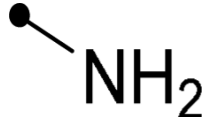
#	R_1	$IC_{50}{}^a$ (μM)
1a		2.6
6a		9.7
5a		10.3
1b		8.8
1c		7.5
1d		6.7
1e		3.2
1f		5.5
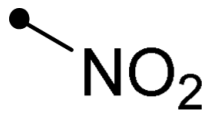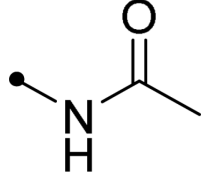
a IC_{50} values were determined with a fluorescent-based assay using CMNGC as a fluorescent reporter substrate (see methods section). Reported IC_{50} values are the average of triplicates with at least two datum points above and at least two below the IC_{50}. The fluorescent-based assay as performed here has a standard error between 10% and 20%, suggesting that differences of two-fold or greater are significant.

Table 2

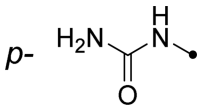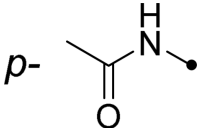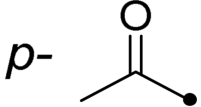Effect of R_2-R_5 moieties on Cif inhibitory potency
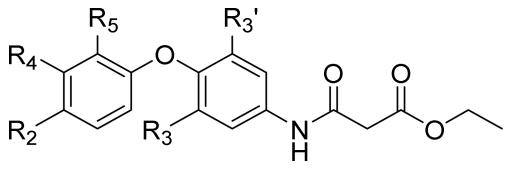
#	R_2	R_3	R_4	R_5	$IC_{50}{}^a$ (μM)
1d	OH	$R_3=R_3'=Br$	Isopropyl	H	6.7
1g	H	$R_3=R_3'=Br$	Isopropyl	H	>50
1h	OCH_3	$R_3=R_3'=Br$	Isopropyl	H	>25^b
1i	OH	$R_3=R_3'=Cl$	Isopropyl	H	3.8
1j	OH	$R_3=Cl, R_3'=H$	Isopropyl	H	11.6
1k	OH	$R_3=R_3'=Cl$	H	H	>50
1l	OH	$R_3=R_3'=Cl$	Br	H	4.9
1m	OH	$R_3=R_3'=Cl$	I	H	3.8
1n	OH	$R_3=R_3'=Cl$	CF_3	H	3.0
1p	OH	$R_3=R_3'=Cl$	Ethynyl	H	2.9
1q	OH	$R_3=R_3'=Cl$	H	Br	29.3

^{a}IC_{50} values were determined with a fluorescent-based assay using CMNGC as a fluorescent reporter substrate (see methods section). Reported IC_{50} values are the average of triplicates with at least two datum points above and at least two below the IC_{50}. The fluorescent-based assay as performed here has a standard error between 10% and 20%, suggesting that differences of two-fold or greater are significant.

^{b}Limited by the solubility (25 <S<50 μM) of the compound under assay conditions (1% DMSO, 0.1 mg/mL BSA at 37 °C). Solubility was measured using a previously described method.[29]

Table 3

Inhibitory potency of a series of compounds designed to target the catalytic site of Cif

#	R	IC$_{50}^{a}$ (μM)
8a	H	1.4
8b	*p*-COOH	10.5
8c	*p*-CONH$_2$	0.35
8d	*m*-CONH$_2$	0.46
8e	*p*-CN	11.9
8f	*m*-CN	0.58
8g	*p*-CONHMe	1.7
8h		0.29
8i		15.6
8j		0.35
8k		2.0
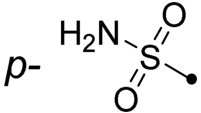
[a]IC$_{50}$ values were determined with a fluorescent-based assay using CMNGC as a fluorescent reporter substrate (see methods section). Reported IC$_{50}$ values are the average of triplicates with at least two datum points above and at least two below the IC$_{50}$. The fluorescent-based assay as performed here has a standard error between 10% and 20%, suggesting that differences of two-fold or greater are significant.

Table 4

Selectivity profiles, *in vitro* metabolic stability and physico-chemical properties of selected compounds

#	1a	8c	8h	8j
TR agonist EC_{50} (nM)	0.43±0.14	>10,000	>10,000	>10,000
TR antagonist (% inhibition at 10 µM)	-	66%	28%	33%
Human sEH IC_{50} (µM)[a]	-	8.6	7.5	7.7
Human mEH IC_{50} (µM)[b]	-	17.2	26.3	97.8
Human liver microsomal stability $t_{1/2}$ (min)	-	15	29	5.7
Stability in cell culture (%)[c]	-	106±8	103±12	74±30
Molecular weight	487	445	460	444
Melting point (°C)	-	261.3-262.0	162.0-162.9	190-194
$LogP$[d]	4.71	4.44	4.11	4.85
Solubility (µM)[e]	-	0.17	21	<0.04
Mouse plasma protein binding[f]	99%	>99%	>99%	>99%

[a]Measured using *t*-DPPO ([3H] *trans*-diphenylpropene oxide) as a substrate, the IC_{50} of 12-(3-adamantan-1-yl-ureido) dodecanoic acid is 16 nM

[b]Measured using CMNGC as a substrate, the IC_{50} of 2-(nonylthio) propanamide is 6.0 µM.

[c]Percentage remaining after 24 h incubation (initial conc:10 µM) with GH3.TRE-Luc cell (mean±SD).

[d]Predicted value using Chembiodraw Ultra 13.0.

[e]Equilibrium solubility measured in sodium phosphate buffer (0.1 M, pH 7.4) without co-solvent nor BSA at room temperature.

[f]Measured at 1 µM using a rapid equilibrium dialysis device (#89809, Thermo Scientific, IL) as described previously[35].